Collisions of UF− 6 ions with Ar, Xe, SF6, and UF6

B. K. Annis and J. A. D. Stockdale

Citation: The Journal of Chemical Physics **74**, 297 (1981); doi: 10.1063/1.440832
View online: http://dx.doi.org/10.1063/1.440832
View Table of Contents: http://scitation.aip.org/content/aip/journal/jcp/74/1?ver=pdfcov
Published by the AIP Publishing

Collisions of UF_6^- ions with Ar, Xe, SF_6, and UF_6

B. K. Annis

Chemistry Division, Oak Ridge National Laboratory, Oak Ridge, Tennessee 37830

J. A. D. Stockdale

Chemical Physics Section, Health and Safety Research Division, Oak Ridge National Laboratory, Oak Ridge, Tennessee 37830

(Received 14 August 1980; accepted 17 September 1980)

Electrostatic energy analysis has been performed on the products of collisions of up to 200 eV (lab) UF_6^- ions with Ar, Xe, SF_6, and UF_6. Negative ions of UF_6 containing internal excitation energy up to ~5 eV have been observed and their distributions as functions of scattering angle and internal excitation recorded. The behavior of the fragment ions F^- and UF_5^- was investigated and found to be in accord with a simple statistical model of the collision dynamics.

I. INTRODUCTION

The UF_6 molecule is known to have a very high electron affinity (E.A.). Ion–cyclotron resonance,[1] collisional ionization,[2–4] and surface ionization[5] experiments support a lower limit of ~5 eV, while calculations have yielded estimates of 5.0,[6] 6.1,[7] and 8.3 eV.[8] Such a large E.A. suggests the possibility of several excited electronic states of the UF_6^- ion. In recent calculations Koelling, Ellis, and Bartlett,[9] Boring and Wood,[10] and Hay, Wadt, Kahn, Raffenetti, and Phillips[8] have estimated the positions of a number of excited states of UF_6^-. They are thought to lie in the region between 0.67 and 2.69 eV above the $^2A_{2u}$ ground state.

Recent studies of collisional ionization of atomic Cs by UF_6 have strongly suggested that the corresponding product UF_6^- is internally excited.[2,4] Energy analysis of the final Cs^+ kinetic energy distributions implies an average excitation of ~3 eV even at the lowest laboratory impact energy of 7 eV.[11] However, the conclusion that highly excited UF_6^- states were involved was indirect since it was based on measurements of Cs^+ distributions and the assumption of a ground state E.A. of ~5 eV for UF_6.

In the present paper we describe the results of a series of experiments designed to check directly for the existence of highly excited UF_6^- ions. We have examined the energy losses of well-defined beams of UF_6^- ions in collision with Ar, Xe, SF_6, and UF_6 static gas targets and also have obtained information on the fragmentation of UF_6^- in such collisions. The results are unambiguous in showing the existence of highly excited UF_6^- with internal excitation up to at least 5 eV but it is difficult to compare the experimental results directly with the theoretical estimates of the UF_6^- excited electronic states.[8–10] A short summary of the energy loss results for UF_6^- collisions with Ar has been presented elsewhere.[12]

II. EXPERIMENTAL

The apparatus used in this study was adapted from that used previously in studies of collisional ionization of alkali atoms by various molecules. Its dimensions, the electrostatic energy analyzer used to inspect both scattered and unscattered UF_6^- beams, and the associated positioning, vacuum, and data handling equipment have been described previously.[13,14] New features of the present arrangement were the UF_6^- source and the gas target cell. The vacuum system consisted, as before, of two separate vacuum chambers connected through a valved port but each with its own pumping system. The ion source was located in the chamber which previously contained the fast neutral–alkali beam source, while the upright cylindrical stainless-steel gas target cell was located in the center of the main collision chamber and was fed by the multichannel hole array previously used to generate a vertical target gas beam.

Negative uranium hexafluoride ions were generated by surface ionization on a hot (850°C) carbon filament. In equilibrium with the hot surface at this temperature UF_6^- ions will have an average of 1.6 eV of rotational and vibrational energy. The likelihood of electronic excitation appears to be less than 1%, given the calculated positions of excited states of UF_6^- (Refs. 8–10) and an E.A. of UF_6 near 5 eV.

A simple extraction and einzel lens system focused the UF_6^- ions upon the 1 mm wide entrance slit of the cylindrical 1.5 cm diam target gas cell which was located 70 cm from the carbon filament. Background pressure in the main vacuum chamber containing the electrostatic analyzer and gas target cell was $\leq 1\times10^{-6}$ Torr with the UF_6^- beam alone, and $< 5\times10^{-5}$ Torr with the gas cell filled. Changes in the target gas pressure were found to have no effect on the energy spectra so that multiple collision effects may be discounted. However, in the present series of measurements we did not attempt to obtain cross sections and the actual target gas pressure was not measured. A Faraday cup attached to a rotatable arm could be moved to intercept the UF_6^- beam 10 cm in front of the target gas cell and beam currents of $\gtrsim 10^{-9}$ A at laboratory kinetic energies of 100 eV and greater were routinely obtained.

The electrostatic analyzer was attached to an arm which could be rotated in the horizontal plane about the center of the gas cell. The 1 mm diam entrance slit to the analyzer was located 15 cm from the center of the target gas cylinder. The latter was provided with a beam exit hole of 3 mm diam so that angular scattering

 0021-9606/81/010297-08$01.00

could be observed out to 5° in the forward laboratory direction. The full width at half-maximum (FWHM) of the UF_6^- beam was measured to be 0.5 eV with an angular spread (FWHM) of 0.5°. The analyzer was operated in the constant transmission mode[13] with an energy resolution of 0.2 eV. Normally, ions were transmitted through it at 40 eV kinetic energy.

Uranium hexafluoride gas, depleted in ^{235}U, was obtained from the Oak Ridge Gaseous Diffusion Plant. It was vacuum distilled through several freeze–thaw cycles and introduced to the source region or target cell through baked out stainless steel lines. Argon, xenon, and SF_6 were Matheson research grade and were similarly introduced to the target cell without further purification. Both the target cell and all apertures and surfaces of the electrostatic analyzer viewed by the incident or scattered UF_6^- beam were spray coated with colloidal graphite. In previous collisional ionization studies in the same apparatus[11] checks were made for contact potentials between the scattering center, then surrounded by a set of gold plates, and the entrance slit of the analyzer. No contact potentials were observed for noble gas or SF_6 targets; however, a contact potential of 1.8 V appeared between scattering center and analyzer when UF_6 was used as a target.[11] In the present study it was not possible to test for a contact potential in the same way. For UF_6 such a contact potential might result in at most an overestimate of the UF_6^- beam energy at collision of something less than 1% for a 200 eV beam and ~2% for a 100 eV beam. Measurements of UF_6^- energy loss relative to the beam peak would be unaffected, as would measurements of the energy interval between negative ions formed in the collision region.

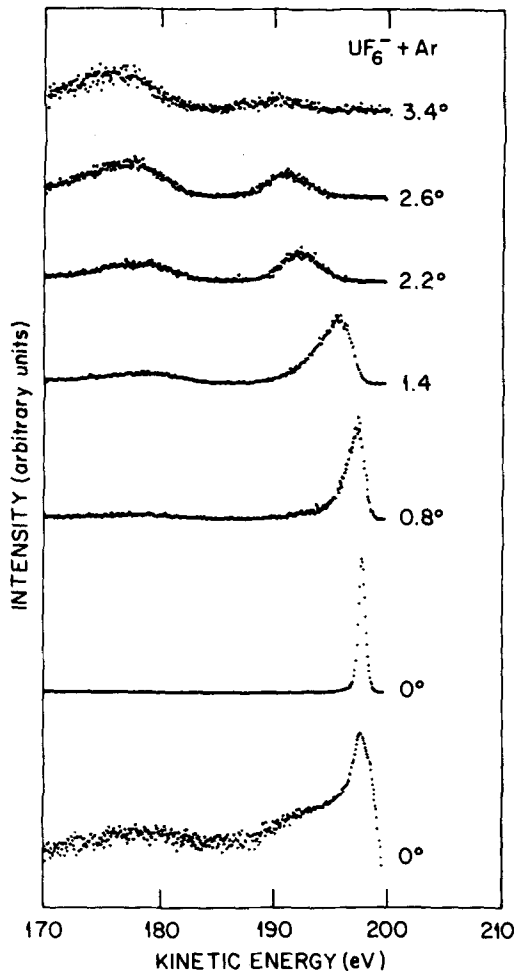

FIG. 1. Kinetic energy spectra of negative ions for collisions of 198.2 eV UF_6^- ions with Ar at various laboratory scattering angles. The two 0° spectra are the same; that at the bottom being displayed with a logarithmic intensity scale; that above it with a linear intensity scale to show the profile of the incident UF_6^- beam. All other spectra have linear intensity scales.

III. RESULTS

Figure 1 shows negative ion energy spectra within the kinetic energy region from 170 to 200 eV as a function of laboratory system scattering angle for collision of a 198.2 eV UF_6^- beam with Ar. The 0° spectrum is shown at the bottom plotted on a log intensity scale. Above, it is replotted on a linear intensity scale as are the spectra at the various scattering angles. In the log intensity plot of the 0° spectrum three features are evident: the main beam itself, a shoulder to the left of it, and a broader peak centered at 179 eV. In the corresponding linear plot only the main beam can readily be seen. The energy loss shoulder and broad peak at 179 eV do not occur in the absence of the scattering gas.

At the other scattering angles shown in Fig. 1 no trace of the main beam was present. The broad lower energy peak gradually becomes more important than the higher energy peak as the scattering angle is increased. Noticeable also is the fact that the higher energy peak moves to larger energy losses as the scattering angle increases. Figure 2 shows an additional low energy feature, peaking near 10 eV, which remains almost constant in energy as the scattering angle increases. These data were obtained under the same conditions as those of Fig. 1. No additional structure was seen in the energy interval between 30 and 170 eV.

Figure 3 shows the results of time-of-flight measurements on the three features visible in the 0° spectrum of Fig. 1. Here the analyzer was set successively to transmit ions at the three points [(a), (b), and (c) shown in the 0° energy spectrum at the bottom of Fig. 3]. Ions were then admitted to the analyzer only during a 0.5 μs time gate applied once each 46 μs and their transit time recorded. A more detailed description of the use of the analyzer as a time-of-flight mass spectrometer has been given elsewhere.[13] From inspection of Fig. 3 it is clear that the transit times of point (b), the higher energy shoulder, and point (c), the main beam, are the same but that the point (a), corresponding to the broad peak near 179 eV, yields ions with a shorter transit time. From earlier mass calibrations and other data similar to Fig. 3 we conclude that the ion group near point (a) is UF_5^- while that near point (b) is UF_6^-. Similar measurements on the low energy peak of Fig. 2 have shown it to be F^- with a small contribution of electrons near zero energy.

Figure 4 shows energy spectra for collisions of near 100 eV UF_6^- with Ar. The 0° spectrum is again dis-

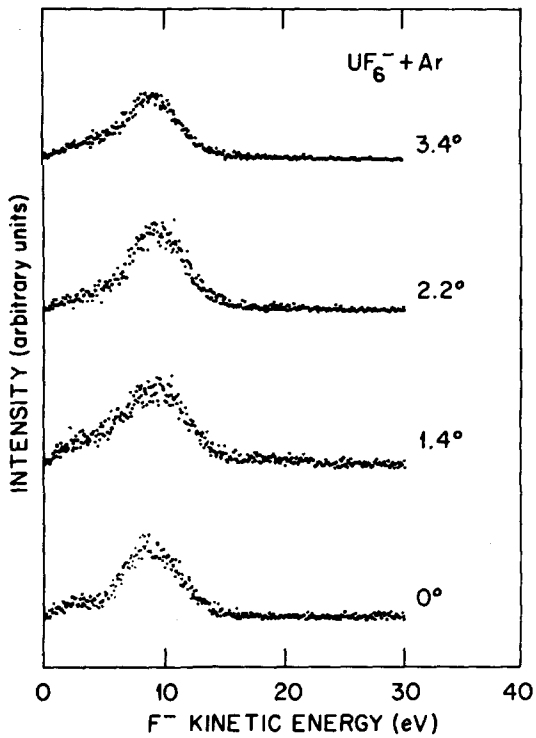

FIG. 2. F^- kinetic energy spectra for impact of 198.2 eV UF_6^- ions on Ar at the laboratory scattering angles shown. The small group to left of main peak is electrons due to stripping on slits and on background gas.

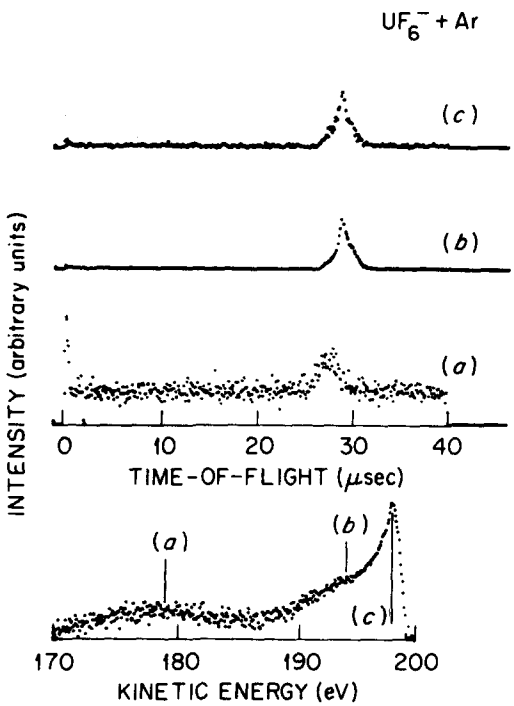

FIG. 3. Identification of negative ions in collisions of 198.2 eV UF_6^- ions with Ar. Bottom spectrum: kinetic energy spectrum of negative ions from 170 to 200 eV in the forward direction. Time-of-flight spectra: (a) time of flight of UF_5^- ions for electrostatic energy analyzer set to transmit ions at point (a) in kinetic energy spectrum; (b) and (c) times of flight of UF_6^-* and UF_6^- ions, respectively, for analyzer set to transmit at points (b) and (c) of the energy spectrum. For details see the text.

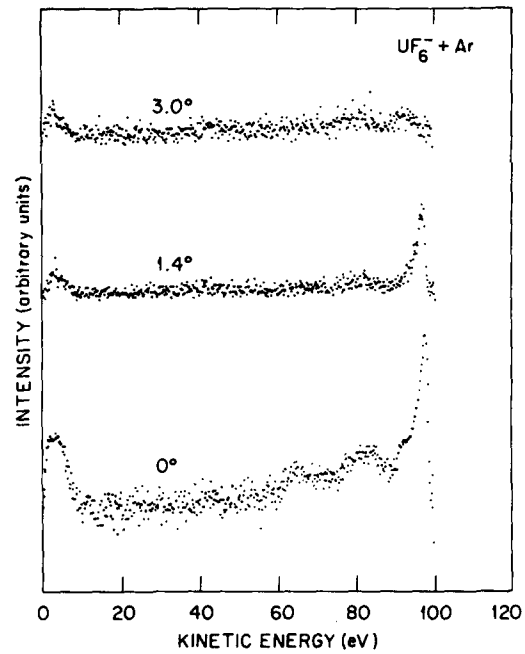

FIG. 4. Kinetic energy spectra for impact of 98.4 eV UF_6^- ions on Ar at the laboratory scattering angles shown. The 0° spectrum is displayed on a log intensity scale; 1.4° and 3.0° are displayed on a linear intensity scale.

played on a log intensity scale, the others on linear. The same general features as seen in Figs. 1 and 2 are apparent with the probable appearance of another peak near 65 eV in the 0° spectrum. Due to its low intensity it was not possible to perform a time-of-flight mass analysis on this feature. Its possible origin will be discussed below.

Figures 5–7 show energy spectra for collisions of UF_6^- with Xe, SF_6, and UF_6, respectively. The features observed in these three figures are very similar to those seen in collisions with Ar. For the Xe case the ion identifications are the same as for Ar. However, we have not been able to perform completely unambiguous time-of-flight mass measurements on the energy loss peaks of Figs. 6 and 7. It is possible that UF_7^- and/or UF_5^- may contribute to the upper peak and that UF_4^- and/or UF_3^- may be involved in the lower energy peak. The similarities in the general shape of these results with those for UF_6^- collisions with Ar and Xe suggest that any such admixtures are probably quite small at the kinetic energies represented by these peaks. However, until unambiguous identification can be performed, their exact composition must remain in doubt. Beauchamp[1] has previously studied reactions of UF_6^- ions produced on a hot (800 °C) Rh filament with a UF_6 gas target for the center-of-mass kinetic energy region from near 0 to 35 eV. Product ions were detected by ion–cyclotron resonance and were confined to those having laboratory kinetic energies of less than 1 eV in the direction of the ion beam. The formation of UF_7^-, UF_6^-, UF_5^-, and UF_3^- was observed and reaction rates for these conditions measured. We can make no direct comparison with these results due to the differing energy regions studied.

IV. DISCUSSION

In what follows we will be concerned with the following four reactions and their interrelationships:

$$UF_6^- + A \rightarrow UF_6^{-*} + A \ , \quad (1)$$

$$UF_6^- + A \rightarrow F^- + A + UF_5 \ , \quad (2)$$

$$UF_6^- + A \rightarrow UF_5^- + A + F \ , \quad (3)$$

$$UF_6^- + A \rightarrow UF_6 + e + A \ , \quad (4)$$

where A stands for Ar, Xe, SF_6, or UF_6. Total cross sections for processes (2)–(4) have recently been reported by Champion *et al.*[15] We will divide the discussion into two parts: production of excited UF_6^- and production of fragment ions.

A. Production of excited UF_6^- ions (UF_6^{-*})

Figure 8 shows Q distributions for the process (1) calculated point by point from those sections of the data shown in Fig. 4 which correspond to formation of UF_6^{-*}. The inelasticity of the process $-Q$ is the quantity of kinetic energy converted into internal energy of excitation of the UF_6^{-*}, as measured from the observed UF_6^{-*} energy distributions. From conservation of energy and momentum, Q is given by the expression

$$Q = E_0\left(\frac{m_1}{m_2} - 1\right) + E^*\left(\frac{m_1}{m_2} + 1\right) - 2\frac{m_1}{m_2}\sqrt{E_0 E^*}\cos\theta \ , \quad (5)$$

where E_0 is the kinetic energy of the UF_6^- beam, E^* the energy of the UF_6^{-*} component after the collision, m_1 the mass of UF_6, m_2 the mass of target atom or molecule, and θ the scattering angle in the laboratory system.

Larger quantities of initial excitation of UF_6^{-*} than shown in Fig. 8 are, of course, possible provided they result in processes (2), (3), or (4) or some other process leading to decay or dissociation of the UF_6^{-*} in a time less than about 45 μs. The latter is the approximate transit time of UF_6^- from the collision region to the detector in the present experiment. The 0° distribution of Fig. 8, and those in subsequent figures as well, were obtained by recording and storing a "background" beam profile in the absence of scattering gas and subtracting this from the profile observed with scattering gas. That section of the resultant clearly corresponding to UF_6^{-*} was then used to calculate the Q distribution.

Figure 9 shows similar Q distributions calculated from the data of Fig. 1 (200 eV UF_6^- on Ar) and Fig. 10

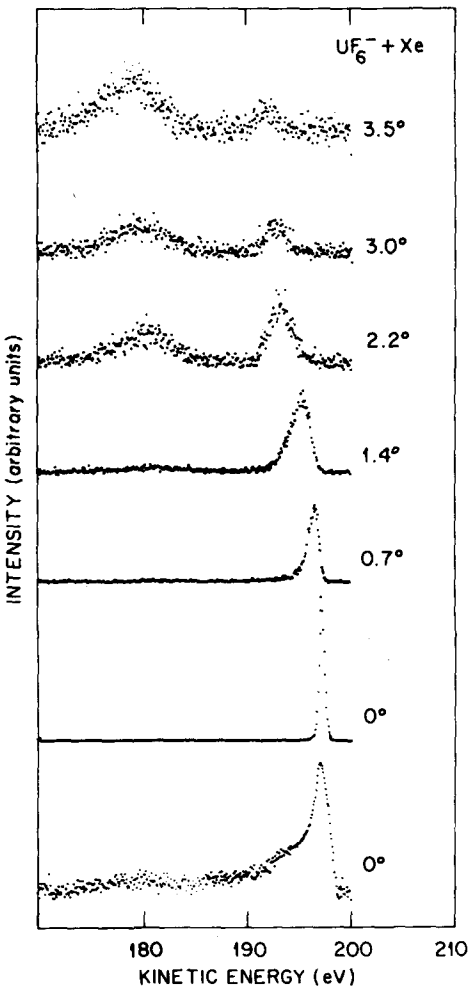

FIG. 5. Kinetic energy spectra for impact of 197.3 eV UF_6^- ions on Xe at various laboratory scattering angles. The two 0° spectra are the same; the lower is displayed on a log intensity scale. All other data are shown on linear intensity scales.

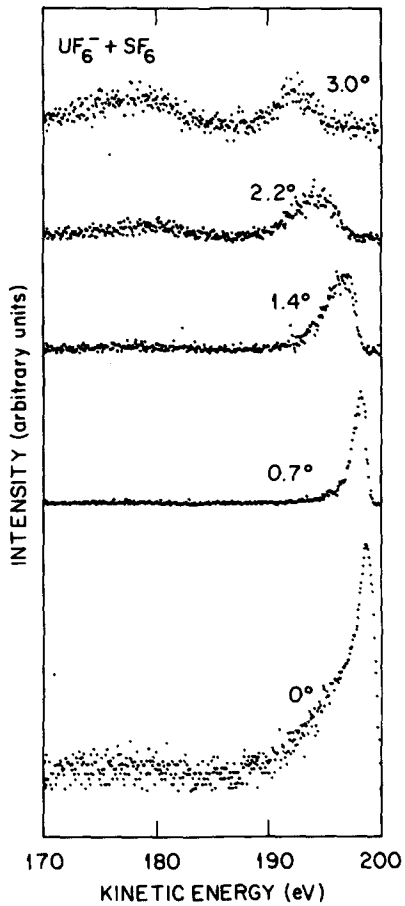

FIG. 6. Kinetic energy spectra for impact of 198.5 eV UF_6^- on SF_6 at various laboratory scattering angles. The 0° spectrum is displayed on a log intensity scale. All other data have linear intensity scales.

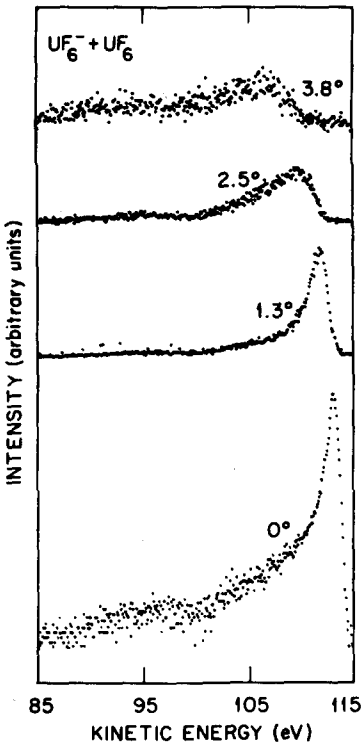

FIG. 7. Kinetic energy spectra for impact of 113 eV UF_6^- on UF_6 at various laboratory scattering angles. The 0° spectrum is displayed on a log intensity scale. All other data have linear intensity scales.

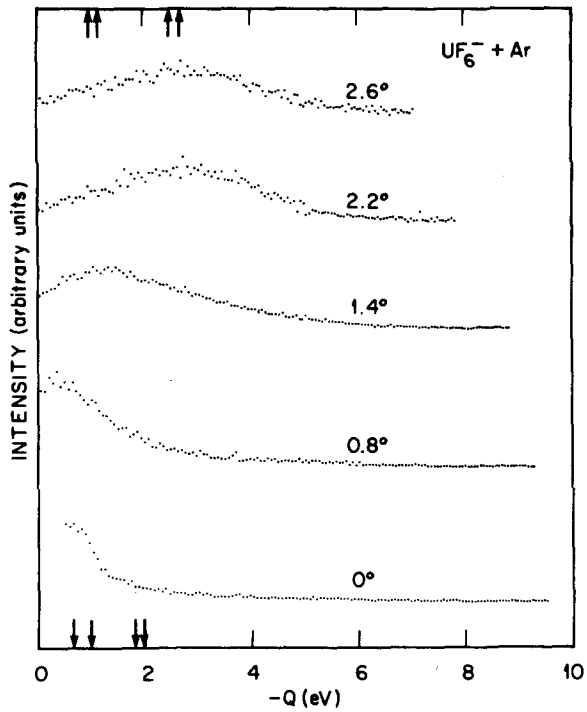

FIG. 9. Plots of $-Q$ against intensity for the inelastic collision UF_6^- (198.2 eV) + Ar → UF_6^-* + Ar. The laboratory scattering angles of 0°, 0.8°, 1.4°, 2.2°, and 2.6° correspond to center-of-mass angles of 0°, 8.2°, 15°, 24°, 28°, and 40.5°, respectively. Arrows at the bottom and top indicate calculated positions of UF_6^- excited electronic states from Refs. 8 and 9, respectively.

shows similar results for the process (1) obtained from the 200 eV UF_6^- + Xe data shown in Fig. 5. Evident in all three of Figs. 8–10 is an increase in $-Q$, i.e., in the state of excitation of the UF_6^-*, as the scattering angle increases. This increase in inelasticity is in accord with the notion that a greater change in trajectory results from an increased loss in kinetic energy. Such a trend has been noted in positive ion scattering.[16] Also noteworthy is the similarity of the distributions for collisions with Ar and Xe. It is important to note that, except for the 0° distribution, the center-of-mass system scattering angles are different in Figs. 9 and 10 so that some degree of interpolation is required to compare the Q distributions. The center-of-mass scattering angles are given in the figure caption.

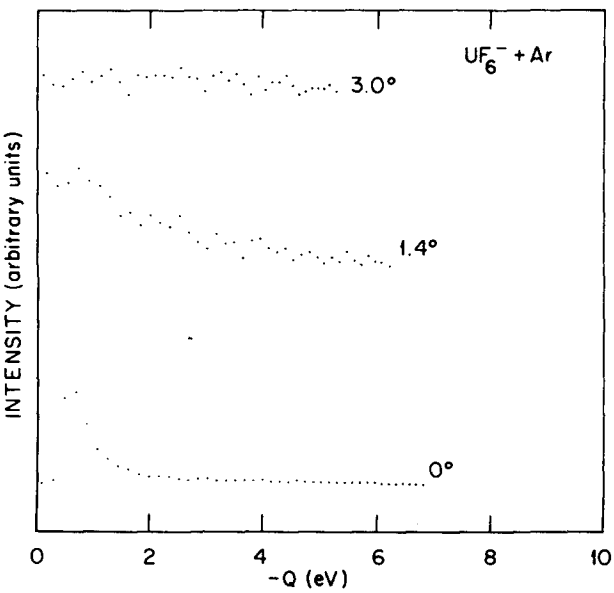

FIG. 8. Plots of $-Q$ against intensity for the inelastic collision UF_6^- (98.4 eV) + Ar → UF_6^-* + Ar at the laboratory scattering angles shown.

Figures 8–10 show that the Q distributions fall to near zero between 5 and 6 eV. Since the lowest metastable levels of Ar and Xe occur at 11.55 and 8.32 eV, respectively, it is clear that these distributions correspond to excitations of UF_6^-. Further, they indicate that processes such as Reactions (2)–(4), or autodetachment of the electron

$$UF_6^- + A \rightarrow UF_6^-{}^* + A \rightarrow UF_6^{(*)} + e + A \qquad (6)$$

must occur once the internal level of excitation of the UF_6^-* exceeds about 6 eV. This is consistent with the earlier estimates of an E.A. of UF_6 in the region from 5 to 6 eV,[1–7] but probably not with estimates as high as 8 eV.[8] It must be borne in mind, however, that the Q distributions represent only internal energy acquired by the UF_6^- in the collision. Due to its formation on a hot filament at 850°C, a UF_6^- molecule may arrive at the collision point with an average internal energy of 1.6 eV provided it has not radiated on its 70 cm flight path. The UF_6^-* ions produced in the collision may therefore actually contain 1.6 eV additional energy of excitation on the average, over and above that indicated by the Q distributions.

The relativistic discrete variational calculations of Koelling, Ellis, and Bartlett[9] for the position of the four lowest electronically excited states of UF_6^-, designated Γ_{8u}, Γ_{7u}, Γ_{8u} and Γ_{6u} in ascending order of energy, are indicated by arrows at the top of Figs. 9 and 10. The relativistic effective-core-potential calculations of Hay *et al.*[8] are shown similarly by arrows at the bottom. The observed Q's span these states but no obvious structure correlating with their positions can be seen. This is understandable since the UF_6^{-*} is probably highly excited vibrationally, which would tend to smear out any sharp peaks.

Figures 11 and 12 show Q distributions corresponding to formation of UF_6^{-*} in collisions with SF_6 and UF_6, respectively. They are derived from the data of Figs. 6 and 7. The masses of Xe (131) and SF_6 (146) are similar so that the distributions for similar laboratory scattering angles can reasonably be compared. The four Q distributions of Fig. 12 can also be compared, in order, with the lowest four distributions of Figs. 10 and 11. The kinetic energy of the UF_6^- beam in Fig. 7, from which the distributions of Fig. 12 were calculated, was chosen so that the scaling factor $(E\theta)_{\text{center of mass}}$, the product of UF_6^- beam energy and scattering angle in the center-of-mass system, is closely comparable between each pair of the lower four distributions of Figs. 11 and 12. Center-of-mass scattering angles are given in the captions to Figs. 10–12. Strictly speaking, the center-

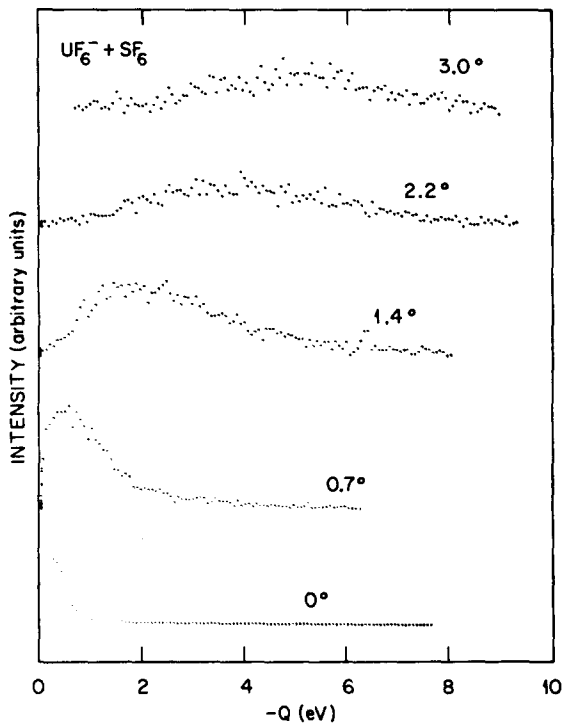

FIG. 11. Plots of $-Q$ against intensity for the process UF_6^- (198.5 eV) + $SF_6 \rightarrow UF_6^{-*} + SF_5^{(*)}$. The laboratory scattering angles of 0°, 0.7°, 1.4°, 2.2°, and 3.0° correspond to center-of-mass angles of 0°, 2.4°, 4.9°, 7.7°, and 10.5°, respectively.

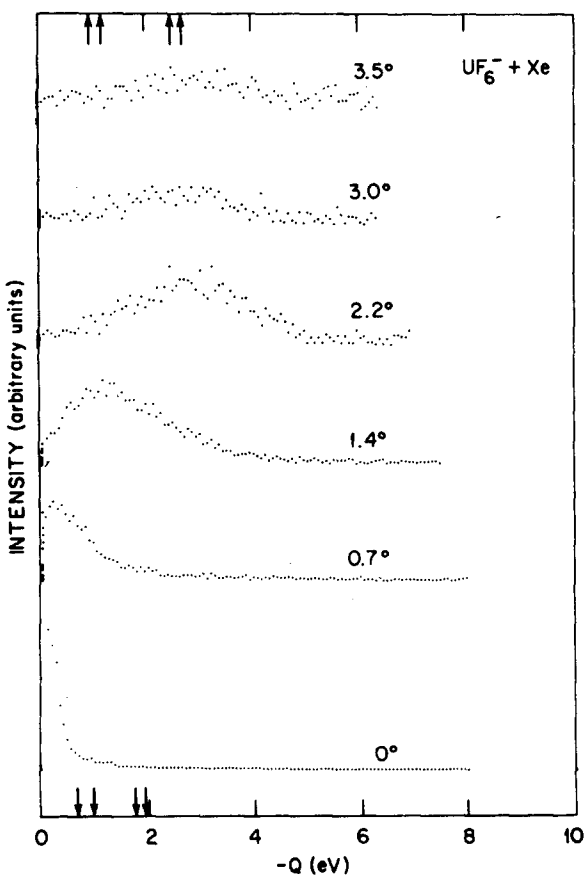

FIG. 10. Plots of $-Q$ against intensity for the inelastic process UF_6^- (197.3 eV) + Xe $\rightarrow$ UF_6 + Xe. The laboratory scattering angles angles of 0°, 0.7°, 1.4°, 2.2°, 3.0°, and 3.5° correspond closely to center-of-mass angles of 0°, 2.6°, 5.3°, 8.3°, 11.5°, and 13.3°, respectively. Arrows at the bottom and top indicate calculated positions of UF_6^{-*} excited states from Refs. 8 and 9, respectively.

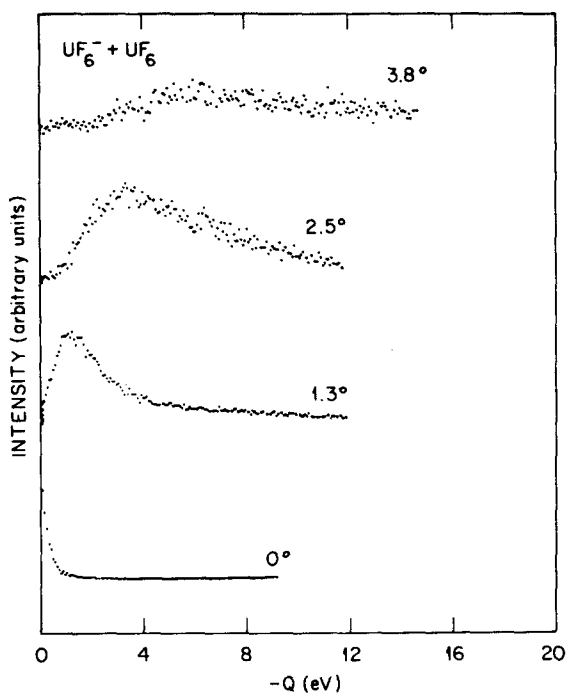

FIG. 12. Plots of $-Q$ against intensity for the process UF_6^- (113 eV) + $UF_6 \rightarrow UF_6^{-*} + UF_6^{(*)}$. The laboratory scattering angles of 0°, 1.3°, 2.5°, and 3.8° correspond closely to center-of-mass angles of 0°, 2.6°, 5.0°, and 7.6°, respectively.

of-mass scattering angle varies for a given lab angle as Q changes. However, this effect is quite small in the present data, amounting to ~0.2° for $UF_6^- + SF_6$ for a Q change of 5 eV. Comparing the lower four distributions of Figs. 10–12, it is obvious that larger values of $-Q$ are involved in collisions of UF_6^- with SF_6 and especially with UF_6 than with the "hard sphere" noble gases. In the case of collisions with UF_6 the $-Q$ distributions peak at values twice those seen in collisions with Xe (or Ar) and also are twice as broad. The situation with SF_6 is less pronounced though the inelasticity of the collision is obviously greater than in the case of Xe or Ar. Evidently, the target SF_6 and UF_6 are also becoming excited in the collision with UF_6^-. In the case of UF_6 where target and projectile probably became indistinguishable during the course of the slow collision, this process becomes very efficient, resulting in a doubling of the inelasticity over the hard sphere case. In some sense we might dub this a "symmetric inelastic collision" as distinct from an asymmetric case where the target and beam are different base species.

One final comment should be made on the small peak evident at 65 eV in the 0° spectrum of Fig. 4. If a UF_6^-* forward scattered peak energy of 96.2 eV, corresponding to a $Q = -2.09$, is taken for the 0° data, we would expect a corresponding backward scattered UF_6^-* peak to occur at 63.7 eV. Alternatively, if a Q of about -7 eV is assumed, then backscattered UF_6^-* which dissociates into UF_5^- could also account for this peak. We have not been able to distinguish a backscattered peak at other angles or other collision energies, or with the other collision partners, though the relevant energy ranges have been examined. We conclude that the cross section for backscattering of UF_6^- is in general very small compared to that for the forward scattering.

B. Dissociation of UF_6

In a recent investigation of collisions of UF_6^- with rare gas targets, Champion *et al.*[15] obtained total cross sections for the dissociation channels which result in F^- and UF_5^- fragments [Eqs. (2) and (3)]. In addition, time-of-flight measurements indicated that a significant fraction of the neutral particles produced in collisions with rare gases could not be correlated with the simple electron detachment process [Eq. (4)]. Although the identity of the neutral particles could not be determined, the results implied that the dissociation channels were of importance. Since these channels involve three particles, it might have been expected that an analysis of the collision dynamics would be intractable. Fortunately, however, a simple two step model represented by

$$A + UF_6^- \rightarrow UF_6^{-*} + a \ ,$$

$$UF_6^{-*} \begin{cases} \nearrow UF_5 + F^- \ , \\ \searrow UF_5^- + F \ , \end{cases}$$

where UF_6^-* is considered to be a complex with internal statistical equilibrium, was found to account for the branching ratios of ion fragment channels and also for the time-of-flight distributions of the neutral fragments.

TABLE I. Intensities of negative ion products due to collisions of 198.2 eV UF_6^- with Ar.

Angle of scatter (deg)		Negative ion intensity at peak (counts/min)			
Lab	Center of mass	UF_6^{-*}	UF_5^-	F^-	F^-/UF_5^-
0	0		6.4	20.2	3.2
0.8	8.2	115	5.8		
1.4	15	28	4.3	15.0	3.5
2.2	24	12.1	7.5	25.8	3.4
2.6	28	6.4	8.7		
3.4	40.5	1.4	4.4	19.8	4.5

Since the latter data were somewhat limited in scope, the present results provide an additional test of the two-step model through the direct observation of the energy and angle distributions as well as mass identification of the ion products.

Table I shows the peak intensities of the UF_6^-, UF_5^- and F^- ion groups from Figs. 1 and 2 normalized to equal accumulation times. The intensities given for θ (laboratory angle of scatter) $\geq 1.4°$ are probably accurate only to within ±50% allowing for a combination of experimental and statistical errors. For $\theta \leq 0.8°$ the accuracy is ±20% with the F^-/UF_5^- peak ratios being accurate to within approximately ±30% for all angles.

Within these limits two trends are apparent. First, the UF_6^-* intensity falls off rapidly with scattering angle. As already seen in the Q distributions discussed in the previous section, this is coupled with an increase in the average internal excitation of the UF_6^-* ion. Secondly, and in contrast to the situation with the UF_6^-* peak, the UF_5^- and F^- intensities do not drop off rapidly with angle. The average F^-/UF_5^- ratio of 3.7 agrees quite well with the ratio of the total cross sections for production of F^- and UF_5^- in UF_6^- collisions with the rare gases reported by Champion *et al.*[15] At the same center-of-mass kinetic energy of 20 eV they obtained a ratio of 3.8. The ratios obtained from Fig. 3 are also in agreement with these authors at the lower center-of-mass energy of 10 eV, as seen in Fig. 4. It is worth mentioning also that, as in the present work, Champion *et al.*[15] reported only the two negative ion production processes (2) and (3) which result in formation of UF_5^- and F^-. The mechanism for production of the observed F^-/UF_5^- ratio will be discussed elsewhere.[17]

Champion and co-workers[15] also measured the total cross section for collisional detachment of the electron and reported that it was less than 1% of the sum of the cross sections of Reactions (2)–(4) in the center-of-mass energy range from 5 to 35 eV. The smallness of this cross section implies that the rapid drop off in the UF_6^-* peak intensity with scattering angle, shown in Table I, cannot be explained by an increasing electron autodetachment probability. Further, autodetachment is largely ruled out since the bulk of the energy loss peak corresponds to Q values less than the probable 5–6 eV E.A.

Within the framework of the RRKM[18] description of complex disintegration the only adjustable parameter available for fitting the energy and angle distributions

TABLE II. Q values deduced from the energy interval between F^- and UF_5^- peaks.[a]

Collision	Kinetic energy (eV) Lab	Kinetic energy (eV) Center of mass	Angle (deg) Lab	Angle (deg) Center of mass	Δ_{exp} (eV)	Q (eV)
UF_6^-+Ar	98.4	10.0	0	0	80	−7
	198.2	20.2	0	0	171	−6
			1.4	17	178	−7
			2.2	24	167	−7.5
			3.4	40.5	167	−4
UF_6^-+Xe	197.3	54.1	0	0	169	−8

[a] Δ_{exp} is the observed difference in the energies of the centers of the UF_5^- and F^- peaks. $-Q$ is the calculated amount of kinetic energy absorbed in the initial impact necessary to reproduce the value of Δ_{exp}.

is $-Q$, the amount of internal energy absorbed by UF_6^- in the impact with the rare gas target. If the two-step model is correct, it should then be possible to vary the value of Q until the location of the peaks observed in the F^- and UF_5^- distributions can be reproduced. Alternatively, Q can be varied to match the energy difference between the F^- and UF_5^- peaks. The latter approach mitigates the effects of any contact potentials which might have been present since both ions would have been affected in the same manner. The Q values obtained from this analysis are listed in Table II and fall in the range 4–8 eV. These Q values, which are in qualitative agreement with those obtained by Champion *et al.*,[17] also reproduce absolute values of the locations of the UF_5^- peaks within the experimental uncertainty. In the case of the F^- peaks, the calculated values differ at most by 2 eV from the observed values. Additionally, Q values in this range reproduce the UF_5^- peaks for the off axis Xe data of Fig. 5 for which F^- data was not obtained.

The RRKM methodology[18] also predicts that a certain fraction of the energy in excess of that required for dissociation [4.7 ± 0.3 eV for $D(UF_5-F^-)$[1] and 4.2 ± 0.3 eV for $D(UF_5^- - F)$[2]] will contribute to relative translational motion of the fragments. This additional kinetic energy causes a broadening of the observed energy distributions. Additional broadening due to apparatus effects will also occur. Since these effects are difficult to characterize, a detailed analysis of the widths of the energy distributions cannot be made. However, it can be said that the range of Q values listed in Table II leads to estimated widths which are all less than the observed values.

In summary, direct measurement of energy and angular distributions combined with mass identification of the fragment ions confirms the conclusions of Champion *et al.*[15,17] that the principal fragment ions produced in collisions of UF_6^- with rare gas targets are F^- and UF_5^- and that the decomposition process is adequately modeled by a two-step hypothesis.

ACKNOWLEDGMENTS

We are grateful to R. L. Champion, L. D. Doverspike, S. Datz, R. J. Warmack, and R. N. Compton for helpful discussions and suggestions and to A. E. Carter for assistance with the experiment.

Research is sponsored by the Office of Health and Environmental Research, U.S. Department of Energy under contract W-7405-eng-26 with the Union Carbide Corporation.

[1] J. L. Beauchamp, J. Chem. Phys. **64**, 939 (1976).
[2] R. N. Compton, J. Chem. Phys. **66**, 4478 (1977).
[3] B. P. Mathur, E. W. Rothe, and G. P. Reck, J. Chem. Phys. **67**, 777 (1977).
[4] B. K. Annis and S. Datz, J. Chem. Phys. **69**, 2553 (1978).
[5] P. F. Dittner and S. Datz, J. Chem. Phys. **68**, 2451 (1978).
[6] M. Boring, Chem. Phys. Lett. **46**, 242 (1977).
[7] N. Bartlett, University of California, Berkeley (private communication quoted in Ref. 2).
[8] P. J. Hay, W. R. Wadt, L. R. Kahn, R. C. Raffenetti, and D. H. Phillips, J. Chem. Phys. **71**, 1767 (1979).
[9] D. D. Koelling, D. E. Ellis, and R. J. Bartlett, J. Chem. Phys. **65**, 3331 (1976).
[10] A. M. Boring and J. H. Wood, J. Chem. Phys. (to be published).
[11] J. A. D. Stockdale, R. J. Warmack, and R. N. Compton, Chem. Phys. Lett. **63**, 621 (1979).
[12] B. K. Annis and J. A. D. Stockdale, Chem. Phys. Lett. **74**, 365 (1980).
[13] R. J. Warmack, J. A. D. Stockdale, and R. N. Compton, Int. J. Mass Spectrom. Ion Phys. **27**, 239 (1978).
[14] R. J. Warmack, J. A. D. Stockdale, and R. N. Compton, J. Chem. Phys. **68**, 1916 (1978).
[15] R. L. Champion, L. D. Doverspike, E. Herbst, S. Haywood, B. K. Annis, and S. Datz, Proceedings of the XI International Conference on the Physics of Electronic and Atomic Collisions, Kyoto, Japan, p. 618 (1979).
[16] S. M. Fernandez, F. J. Eriksen, A. V. Gray, and E. Pollack, Phys. Rev. A **12**, 1252 (1975); J. A. Laramee, P. H. Hemberger, and R. G. Cooks, Int. J. Mass Spectrom. Ion Phys. **33**, 231 (1980).
[17] S. E. Haywood, E. Herbst, L. D. Doverspike, R. L. Champion, B. K. Annis, and S. Datz (to be published).
[18] R. A. Marcus, J. Chem. Phys. **62**, 1372 (1975).